


Fate of Time-Reversal Symmetry Breaking in UTe_2

M. O. Ajeesh¹, M. Bordelon, C. Girod, S. Mishra¹, F. Ronning, E. D. Bauer, B. Maiorov,
J. D. Thompson, P. F. S. Rosa¹, and S. M. Thomas^{1*}

Los Alamos National Laboratory, Los Alamos, New Mexico 87545, USA

 (Received 18 May 2023; revised 13 September 2023; accepted 28 September 2023; published 27 October 2023)

Topological superconductivity is a long-sought state of matter in bulk materials, and the odd-parity superconductor UTe_2 is a prime candidate. The recent observation of a field-trainable spontaneous Kerr signal in UTe_2 at the onset of superconductivity provides strong evidence that the superconducting order parameter is multicomponent and breaks time-reversal symmetry. Here, we perform Kerr effect measurements on a number of UTe_2 samples—grown via both chemical vapor transport and the molten-salt-flux methods—that show a single superconducting transition between 1.6 K and 2.1 K. Our results show no evidence for a spontaneous Kerr signal in zero-field measurements. This implies that the superconducting state of UTe_2 does not intrinsically break time-reversal symmetry. Instead, we observe a field-trainable signal that varies in magnitude between samples and between different locations on a single sample, which is a sign of inhomogeneous magnetic regions. Our results provide an examination of representative UTe_2 samples and place strong constraints on the superconducting order parameter of UTe_2 .

DOI: [10.1103/PhysRevX.13.041019](https://doi.org/10.1103/PhysRevX.13.041019)

Subject Areas: Condensed Matter Physics,
Strongly Correlated Materials,
Superconductivity

I. INTRODUCTION

In a superconductor, electrons form pairs that condense into a macroscopic quantum state with zero electrical resistance. The underlying symmetries of the pair wave function are important to determine the properties of the superconducting state. When the orbital wave function is antisymmetric [$\phi(k) = -\phi(-k)$], an odd-parity superconductivity is realized [1]. When time-reversal symmetry is broken, chiral superconductivity may emerge. Odd-parity chiral superconductors are sought-after materials predicted to host topological excitations with non-Abelian statistics that could enable quantum computing [2,3]. Over the past decade, the search for an odd-parity chiral superconductor has intensified, but an ideal candidate has yet to be established. Sr_2RuO_4 was long thought to be the leading candidate [4], but recent nuclear magnetic resonance experiments showed that the superconducting order parameter is even parity [5].

Odd-parity UTe_2 is a recently discovered chiral superconductor candidate [6]. Evidence for chiral superconductivity in UTe_2 comes from multiple experiments. Scanning

tunneling microscopy reveals an asymmetry in the in-gap surface states at step edges argued to arise from a chiral superconducting state [7]. Microwave surface impedance [8] and anisotropic penetration depth [9] studies also support a chiral superconducting state. In addition, a subset of specific heat measurements found a double peak near the superconducting transition temperature (T_c), which is similar to findings in the chiral superconductor candidate UPt_3 [10–12] and suggests the presence of a multicomponent superconducting state. A key characteristic of a chiral superconductor is that its order parameter breaks time-reversal symmetry, and the polar Kerr effect (PKE) is a powerful probe of time-reversal symmetry breaking. Previous PKE measurements in UTe_2 indeed found a spontaneous Kerr rotation that arises at the onset of superconductivity [13]. Because the Kerr rotation was found to be trainable by cooling in a c -axis magnetic field (B_{1g} symmetry), a $B_{3u} + iB_{2u}$ superconducting order parameter was put forward as the most likely multicomponent state [13]. Further measurements of the PKE under larger training fields revealed that the magnitude of the Kerr rotation (θ_K) scales with the training field up to a certain field, which was attributed to a critical state of magnetic vortices [14].

Importantly, the properties of UTe_2 are markedly sensitive to sample growth conditions. For samples grown via chemical vapor transport (CVT), lower growth temperatures increase T_c from 1.6 K to 2 K [15]. A further decrease in the growth temperature leads to a sudden disappearance of superconductivity and a drastic decrease

*smthomas@lanl.gov

Published by the American Physical Society under the terms of the Creative Commons Attribution 4.0 International license. Further distribution of this work must maintain attribution to the author(s) and the published article's title, journal citation, and DOI.

in the residual resistivity ratio (RRR). CVT growth either at higher temperatures or near the low-temperature limit often leads to samples with an apparent double transition in specific heat [16]. The determination of the origin of the double transition has been hampered by strong sample dependence of the superconducting state of UTe_2 . However, several studies now suggest that, unlike UPt_3 , the double transition is not an intrinsic feature but rather a consequence of sample inhomogeneity [17,18]. Further, single-transition samples show no evidence for a splitting of the superconducting transition under B_{1g} shear stress that couples to the proposed $B_{3u} + iB_{2u}$ order parameter [19], suggesting that the superconducting order parameter may be a single component or belong to different symmetry channels. More recently, the quality of UTe_2 single crystals was further improved using a molten-salt-flux (MSF) growth technique [20], leading to RRRs as large as 1000 and enabling the first observation of de Haas–van Alphen oscillations in UTe_2 [21].

A key outstanding open question is whether a spontaneous Kerr rotation persists in samples that show a single T_c . PKE experiments to date have only been reported on a sample with a double transition near 1.55 K in specific heat [13,14]. In these samples, a large residual specific heat (γ^*) was observed in the superconducting state [6], which has been shown to decrease as T_c is increased [15,18,22]. Notably, a correlation has been identified between the volume fraction of inhomogeneous magnetic clusters detected by muon spin resonance (μSR) and the size of γ^* [23], which naturally points to the role of magnetism in samples with large γ^* .

Here, we investigate the polar Kerr effect on a number of samples grown via both the CVT and molten-salt methods. All samples have only a single detectable transition in specific heat. Our measurements do not show evidence for a spontaneous PKE effect that emerges at T_c in zero-field-cooled measurements. Nonetheless, we observe a field-trainable signal that persists up to T_c and whose magnitude varies significantly between different samples and between different spots on the same sample. Contrary to the correlation observed in μSR [23], no clear trend is observed between the magnitude of the PKE and γ^* , which suggests that magnetic clusters may not be the only source of PKE. The ac susceptibility measurements on another representative set of samples indicate a correlation between T_c and the size of the vortex peak effect, a measure of crystalline quality. This result unambiguously shows that lower- T_c samples have a higher density of vortex pinning centers. Our results demonstrate that UTe_2 does not have a time-reversal symmetry breaking (TRSB) superconducting order parameter and that the inhomogeneous field-trainable PKE has an extrinsic origin.

II. RESULTS

Temperature-dependent specific heat measurements for each of the samples on which PKE was measured, shown in

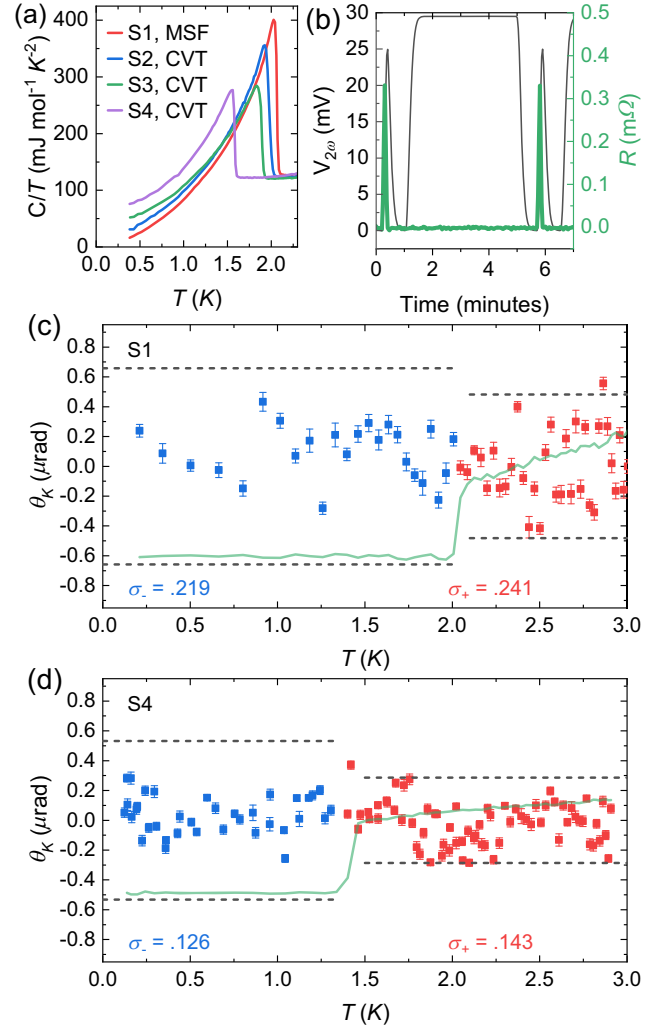


FIG. 1. (a) Specific heat of samples S1–S4. (b) Example of laser pulse sequence used to heat the sample above T_c . The left axis shows $V_{2\omega}$ (proportional to light received by the detector), and the right axis shows the sample resistance. (c,d) Measured value of θ_K as a function of temperature for sample S1 and S4, respectively. The sample is heated above T_c to allow for the possibility of different domain configurations between each data point. Red indicates $T > T_c$; blue indicates $T < T_c$. The faint green line shows the sample resistivity. The dashed lines indicate the expected increase in σ below T_c based on the observation in Wei *et al.* (see text) [14].

Fig. 1(a), reveal a single superconducting transition with a transition width of approximately 50 mK. Note that T_c varies from a minimum of 1.6 K in sample S4 to a maximum of 2.1 K in sample S1. Samples S2–S4 were grown via chemical vapor transport [15], whereas sample S1 was grown using the molten-salt-flux method [20]. As observed previously, the γ^* decreases dramatically as T_c increases [15,18,22], and the MSF sample exhibits the smallest γ^* of only $6 \text{ mJ mol}^{-1} \text{K}^{-2}$ [20]. Table I summarizes the key properties of the samples investigated here. Note that sample S4 has a RRR of 47, which is comparable

TABLE I. Properties of samples studied via PKE, including sample name, growth method, superconducting transition temperature, the size of the specific heat jump at T_c , the residual specific heat determined from a linear fit of C/T versus T^2 , and the residual resistivity ratio (see text).

Sample	Growth method	T_c (K)	$\Delta C/T_c$ (mJmol ⁻¹ K ⁻²)	γ^* (mJmol ⁻¹ K ⁻²)	RRR
S1	MSF	2.1	266	6	400
S2	CVT	2.0	232	21	111
S3	CVT	1.9	163	41	79
S4	CVT	1.6	154	61	46

to the RRR range of 35–40 reported for the samples studied by Hayes *et al.* [13]. This is of relevance because impurity scattering is one mechanism for the observation of a finite PKE arising from a chiral superconducting state [24,25].

Figures 1(c) and 1(d) show the temperature-dependent polar Kerr rotation of our zero-field cooling experiments for samples S1 and S4, respectively. To ensure zero-field cooling conditions, each sample was heated above T_c using a high-intensity light pulse as shown in Fig. 1(b) (see Sec. V for details). Each data point in Figs. 1(c) and 1(d) represents the mean of θ_K measured after the sample is cooled to the indicated temperature from higher temperature ($T \geq T_c$). Data for S2 and S3 are shown in Supplemental Material [26], Fig. S1. No evidence for a spontaneous Kerr rotation below T_c is found for any of the investigated samples.

Under zero-field conditions, prior measurements found that a spontaneous Kerr rotation developed below T_c with amplitude less than or equal to $0.4 \mu\text{rad}$ (ϕ_0) [13,14]. The Kerr rotation was also found to change sign and amplitude between different runs. These changes were attributed to different chiral domain configurations that can form as the sample is cooled through T_c . In the presence of random domains, the standard deviation of the spontaneous Kerr rotation between cooldowns (σ_S) is related to the ratio of

the beam diameter (w) to the average domain size (d) via the expression $\sigma_S = \phi_0 d/w$ for $d < w$, wherein ϕ_0 is the amplitude of the PKE arising from a single domain [27]. The zero-field-cooled data presented by Wei *et al.* [14] have a standard deviation (σ) of $0.097 \mu\text{rad}$ for $T > T_c$ and $0.244 \mu\text{rad}$ for $T < T_c$ across six runs. Assuming that the noise (scatter) in the data (σ_N) and the magnitude of the spontaneous Kerr signal are independent, we find

$$\begin{aligned} T > T_c: \sigma_+^2 &= \sigma_N^2, \\ T < T_c: \sigma_-^2 &= \sigma_N^2 + \sigma_S^2. \end{aligned} \quad (1)$$

This result provides a value for σ_S of $0.224 \mu\text{rad}$, and an approximate domain size of $6 \mu\text{m}$ using the value of ϕ_0 above and the stated beam diameter of $10 \mu\text{m}$. The beam diameter used in this study was also $10 \mu\text{m}$ in diameter.

The values of σ_+ and σ_- were calculated for each sample in this study. In contrast to prior reports [13,14], there is no significant difference between the standard deviation above and below T_c . Using our normal-state deviation σ_+ and the value of σ_S determined from Wei *et al.* [14] would imply a standard deviation in the superconducting state σ_- of 0.329 and $0.226 \mu\text{rad}$ in our data for samples S1 and S4, respectively. Such an increase, illustrated by the $\pm 2\sigma$ dashed gray lines in Figs. 1(c) and 1(d), is not observed.

Although there is no spontaneous Kerr rotation below T_c , all samples show a field-trainable Kerr signal that vanishes at T_c . Figure 2(a) shows the temperature dependence of θ_K for S3 when warmed in zero field after being cooled through T_c in small magnetic fields. A finite Kerr signal clearly emerges for $T < T_c$, and the size of the signal is proportional to the cooling field for fields up to ± 200 Oe. At higher fields, the signal begins to saturate as indicated by the identical Kerr rotation between the curves at 350 and 500 Oe.

In Wei *et al.* [14], θ_K was also found to be proportional to the cooling field. In that study, however, θ_K was always $\pm 0.4 \mu\text{rad}$ for cooling fields between 15 Oe and 30 Oe in magnitude, with the sign of θ_K dependent on the sign of the

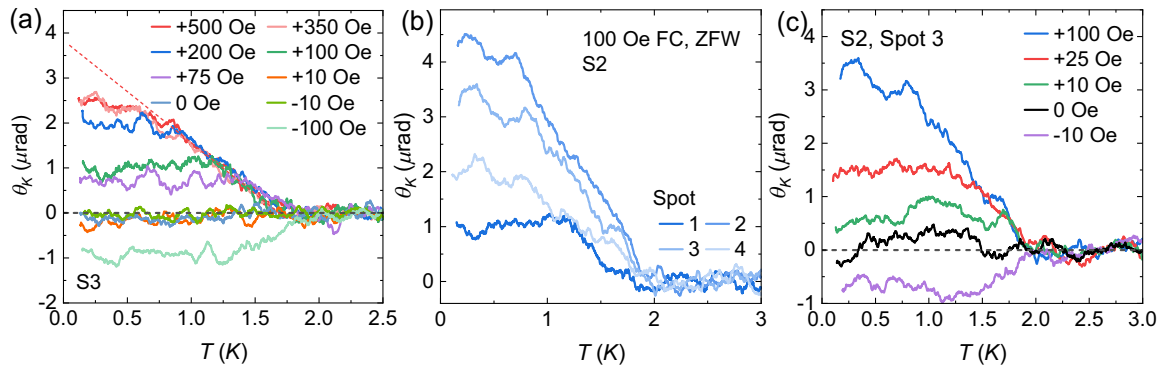


FIG. 2. (a) Zero-field-warmed θ_K after cooling in the indicated field for spot 2 on S3. (b) Zero-field-warmed θ_K after cooling in $+100$ Oe for four different spots on S2. (c) Zero-field-warmed θ_K after cooling in the indicated field for spot 3 on S2. In all cases, the field was applied along the c axis.

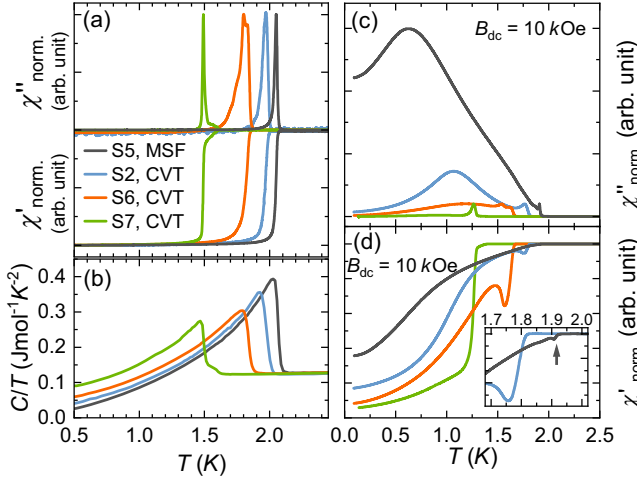


FIG. 3. Specific heat and ac susceptibility on four samples with T_c ranging from 1.48 K to 2.1 K. Sample S2 is the same sample on which the Kerr effect was measured above. (a) Normalized ac susceptibility versus temperature at zero magnetic field with an ac field of 0.25 Oe at 733 Hz. Here, χ' represents the in-phase component and is normalized to a value of -1 at base temperature, whereas χ'' is the out-of-phase component and is normalized to $+1$ at the maximum value. (b) Specific heat versus temperature. (c) Normalized out-of-phase and (d) in-phase components of ac susceptibility cooled in a 10-kOe applied field. The inset of panel (d) shows a zoomed-in view near T_c of S5. Note that χ' is normalized according to the measurement in zero field [panel (a)], and χ'' is normalized to $+1$ at the peak that indicates the onset of superconductivity. For both panels (c) and (d), an ac field of 2 Oe at 733 Hz was applied. All fields were applied along the a axis.

training field. For fields lower than ± 15 Oe, θ_K was distributed between $-0.4 \mu\text{rad}$ and $+0.4 \mu\text{rad}$ as noted above. Thus, aside from the low-field behavior, our results are consistent with those reported in Ref. [14].

Now, we turn to signs of sample inhomogeneity revealed by PKE measurements. Figure 2(b) shows the temperature evolution of θ_K on four different spots of sample S2, upon warming up in zero field after being cooled in a field of $+100$ Oe. As illustrated by Fig. 2(b), there is more than a factor of 4 change in the size of θ_K between the spots measured in sample S2. This inhomogeneity strongly suggests an extrinsic origin for the trainable Kerr effect in UTe_2 . In addition, Fig. 2(c) shows θ_K for spot 3 on S2 when warmed in zero field after being cooled in small magnetic fields. Even in small fields ($< \pm 30$ Oe), θ_K is proportional to the training field. This is in contrast to the behavior previously observed in samples that show a double transition in specific heat, where it was claimed to be due to measuring a single chiral domain [13,14].

To further correlate the PKE behavior with sample quality, we investigate vortex pinning effects through ac magnetic susceptibility measurements. Figure 3(a) presents the real and imaginary parts of the ac magnetic susceptibility $\chi' + i\chi''$ of four different UTe_2 single crystals with a

range of T_c values between 1.48 K and 2.1 K. The specific heat data obtained on the same samples are shown in Fig. 3(b) for comparison. The temperatures of the diamagnetic drop in χ' and the dissipation peak in χ'' are both consistent with the specific heat data. Samples S5, S6, and S2 exhibit a single thermodynamic transition, whereas sample S7 shows two clear transitions at 1.64 K and 1.48 K. Note that sample S2 is the same sample S2 on which PKE data were presented above. Once again, γ^* decreases systematically for samples with higher T_c . Although it has previously been argued that the double transition in some UTe_2 crystals is an intrinsic feature [13], it most often appears in crystals with lower T_c or grown via CVT near the edge of the growth stability region for UTe_2 [16].

To investigate whether lower- T_c samples also have lower crystalline quality, Figs. 3(c) and 3(d) show ac susceptibility measurements cooled in a dc field of 10 kOe applied along the a axis with an applied ac field (h_{ac}) of 2 Oe. Comparing the samples as T_c increases, the relative drop in χ' below T_c decreases for a fixed magnetic field. This apparent trend in the reduction of superconducting screening going from lower- to higher- T_c samples can be attributed to the decrease in the critical current density (J_c) arising from the improved sample quality. We recall that, within the critical state model, H^* is defined as the field at which magnetic flux first penetrates into the center of the sample after zero-field cooling [28,29]. For similar geometry as the samples measured here, H^* near zero temperature is expected to be on the order of 1000 Oe for the lowest T_c (highest J_c) samples [14,30]. In the presence of an applied dc field larger than H^* , the low-temperature $\chi' \propto -J_c/h_{ac}$ [31]. Thus, the lower value of χ' near base temperature in higher- T_c samples is a reflection of the relatively smaller critical current and, therefore, better sample quality.

The relationship between vortex pinning strength and T_c can be seen more clearly in the imaginary part of the susceptibility (χ''), which reveals a peak effect characteristic of vortex lattice dynamics within the mixed state of type-II superconductors [31]. A broad peak in χ'' is observed below T_c due to dissipation from vortex dynamics. As vortex pinning becomes stronger, the broad peak in χ'' decreases due to a decrease in dissipation. Thus, the smaller peak in χ'' is further evidence of stronger vortex pinning in lower- T_c samples.

III. DISCUSSION

The absence of a spontaneous polar Kerr effect in our investigation of representative single- T_c UTe_2 samples requires a careful discussion of consistency checks. First, we note that the size of putative chiral domains should likely increase with increasing sample quality [2]. In the case where the domain size is large compared to the beam diameter, σ_S will equal ϕ_0 ($0.4 \mu\text{rad}$). Our ac-magnetic-susceptibility results demonstrate that higher- T_c samples

have fewer defects, and the spontaneous polar Kerr response should therefore be even higher in the samples measured here if it were an intrinsic effect.

Second, we consider the effects of remanent magnetization in a type-II superconductor after cooling in a constant field and removing the field at base temperature. Clem and Hao [29] have calculated the expected remanent magnetization as a function of vortex pinning strength. In a superconductor with strong vortex pinning, the remanent magnetization is expected to be nearly constant near the center of the sample and to decrease near the edges over a length scale determined by the vortex pinning strength. Near the center, the remanent magnetization is expected to be nonzero up to the irreversibility temperature (T_{irr}), which has been shown to be very close to T_c in UTe_2 for small magnetic fields [32]. Although remanent magnetization has been measured in UPt_3 and URu_2Si_2 [33], prior measurements of θ_K in these systems have not found a signal that scales with the magnitude of the training field [11,34]. It was argued that the reason for the difference between UTe_2 and other U-based materials is that in UTe_2 the vortices carry a magnetic moment [14].

If this were the case, and the observed Kerr effect in UTe_2 was due solely to remanent magnetization or unusual vortex properties, one would expect that θ_K would be uniform across a large region in the center of the sample because of the relatively strong vortex pinning [29]. Our position-dependent PKE measurements in sample S2, however, reveal a significant variation in the magnitude of θ_K as the spot is scanned toward the center of the sample [see Fig. 2(b)]. Because this spatial inhomogeneity in the field-trainable Kerr signal is not fully determined by the bulk remanent magnetization caused by pinning, our result suggests that there is a strong local variation in the vortex distribution. Note that all samples exhibit spot dependence of the field-trainable PKE at a given training field (see Supplemental Material [26], Fig. S6) but that S2 had the largest variation of all measured samples.

One possibility is that the spatial variation in magnitude of the field-trainable PKE is related to sample inhomogeneity on the micron length scale. Previous μSR measurements detected fluctuating magnetic clusters [23] (the volume of which scales with γ^*), and these fluctuations may be pinned by defects to become locally static [35]. In this case, one may expect a direct correlation between γ^* and the size of the Kerr signal at a given training field. Instead, the CVT sample with the lowest γ^* (S2) has the highest variability of θ_K . An obvious distinction between PKE and μSR is that μSR is a bulk probe whereas PKE is surface sensitive. From temperature-dependent optical conductivity measurements, the penetration depth for 1550-nm light is estimated to be only 300 nm [36]. In addition, PKE probes a small surface area (approximately 10 μm diameter) and will therefore depend on the local defect structure. This may lead to a PKE signal that

depends strongly on the proximity of the beam with respect to a pinning center. The PKE measurements on S2, therefore, may have been in a region of the sample that happened to have a larger amount of magnetic clusters even though the total volume of magnetic clusters is lower in S2 compared to the other CVT samples. Future studies of spatially resolved PKE would be useful to test this possibility.

Third, we note that the saturation of θ_K in the highest-quality sample (S1, $T_c = 2.1$ K) occurs between 25 and 100 Oe, whereas a higher field between 200 and 350 Oe is required to saturate θ_K in sample S3 ($T_c = 1.9$ K). It was previously argued that the field where saturation occurs is related to H^* , which is the field where the magnetic flux would first penetrate into the center of the sample after zero-field cooling [14]. At first sight, this decrease in the necessary field for saturation appears to be consistent with the model of Clem and Hao, where H^* is expected to decrease as the vortex pinning strength decreases [29]. The remanent magnetization, however, is also expected to scale with the vortex pinning strength. If the magnitude of θ_K were related to the remanent magnetization of the bulk, then it should decrease as sample quality is improved. Instead, it varies between spots on given samples and between samples with no apparent trend. Thus, the field-trainable PKE is related to remanent magnetization, but there is high spatial variability due to some additional extrinsic properties of the crystal.

A significant difference between samples measured here and in prior reports is whether they host two transitions in specific heat. As has been shown by several studies [15,17,18], the double transition is not an intrinsic feature of UTe_2 . Further, no evidence for a splitting of T_c was found under shear uniaxial stress that would couple to the proposed $B_{3u} + iB_{2u}$ superconducting order parameter [19]. In the face of our results, a plausible explanation for the difference in spontaneous Kerr signals between samples showing either a single or double transition is that the spatial inhomogeneity of the superconducting state in samples showing two transitions may help trap the magnetic flux from fluctuating magnetic clusters and vortices. In addition, extended crystallographic defects (e.g., line dislocations and grain boundaries) provide a natural explanation for stronger vortex pinning in lower- T_c samples, and recent scanning SQUID measurements reveal that vortices tend to form along extended defects [35].

Finally, we discuss the implications of our results for the superconducting order parameter of UTe_2 . If the superconducting state in UTe_2 does not break time-reversal symmetry, proposals in favor of a chiral order parameter must be reevaluated. Aside from PKE measurements [13,14], a chiral order parameter has also been suggested from the temperature dependence of magnetic penetration depth measurements on both CVT- and MSF-grown samples that indicate multiple pairs of point nodes [9].

In contrast, recent scanning SQUID measurements of superfluid density are consistent with a single-component A_{1u} or B_{3u} order parameter [35]. In those measurements, no evidence for chiral domains or half-flux quantum vortices was observed. Other reports that support a chiral order parameter rely heavily on the observation of a TRSB order parameter to rule out other possibilities [7,8]. As mentioned above, there is no evidence for a splitting of T_c under shear uniaxial strain [19]. Further, recent ultrasound measurements provide strong support for a single-component order parameter [37], and no evidence for TRSB was observed in μ sr measurements on high-quality MSF samples [38]. Without direct evidence for a TRSB order parameter, we therefore must conclude that a chiral order parameter in UTe_2 is unlikely.

IV. CONCLUSION

In summary, we performed systematic polar Kerr effect and ac magnetic susceptibility measurements on representative UTe_2 crystals of different qualities to investigate the interplay between sample quality and time-reversal symmetry breaking. Our results show that samples with a single thermodynamic superconducting transition do not develop a spontaneous Kerr rotation in the superconducting state. In addition, the field-trainable Kerr effect observed in these samples is inhomogeneous and sample dependent. We conclude that the superconducting state does not break time-reversal symmetry, and a chiral order parameter is unlikely in UTe_2 .

V. MATERIALS AND METHODS

The UTe_2 samples were grown via both chemical vapor transport [15] and molten-salt-flux [20] techniques. One noted drawback of the MSF technique is the potential inclusion of ferromagnetic U_7Te_{12} with an ordering temperature of 48 K [39] or other uranium-tellurium binaries with ordering temperatures near 115 K [40]. In sample S1, which was grown by the MSF method, ferromagnetic impurities ($\theta_K \approx 1$ mrad) were found on the surface, even after polishing; they tended to grow in thin strips along the a axis. The presence of ferromagnetic impurities was also confirmed by measurements of magnetic susceptibility.

The ac susceptibility was measured in a set of commercially wound, compensated susceptibility coils. Note that the data are normalized with respect to the height of the peak in χ'' at T_c for each sample, which allows comparison between samples of different sizes. The effectiveness of this normalization is shown in Supplemental Material [26], Fig. S7, where two pieces of sample S2 of different size were measured and seen to have similar behavior after this normalization.

Specific heat was measured using the quasi-adiabatic thermal relaxation technique in a He-3 cryostat insert. Both small-pulse and long-pulse methods were used to ensure

that all samples measured only had a single transition in specific heat. Electrical resistivity was collected with a Lakeshore 372 AC bridge using a standard four-probe configuration wherein Pt wires were attached to sputtered gold pads with silver paint. The residual resistivity ratio was determined by fitting the low-temperature resistivity to $\rho(T) = AT^2 + \rho_0$ and taking the ratio $\rho(300 \text{ K})/\rho_0$.

PKE measurements were performed using a fiber-based, zero-area, Sagnac interferometer operating at a wavelength of 1550 nm [27,41]. For more information on this technique as well as a comparison with other probes sensitive to TRSB, see Refs. [42–45]. Samples were mounted on a set of XYZ cryogenic piezo-stepper devices and thermally anchored to the base plate of an adiabatic demagnetization refrigerator. Two different measurement types were performed: (i) heat-pulse experiments to look for the development of a spontaneous PKE below T_c , and (ii) field-cooled, zero-field-warmed measurements to investigate the field-trainable Kerr effect.

An example of the measurement process for the heat pulse experiments (i) is shown in Fig. 1(b). To determine whether a spontaneous PKE onsets at T_c , samples were first cooled under zero magnetic field and illumination. Maintaining zero-field conditions, a high-intensity laser pulse was applied to the sample to heat the sample above T_c . The left axis of Fig. 1(b) shows $V_{2\omega}$, which is proportional to the light received by the photodetector. The initial spike in $V_{2\omega}$ is caused by the high-intensity laser pulse that is used to heat the sample. It does not reach a very large value in the plot because of the short pulse time (7 seconds) compared to the settling time of the lock-in amplifier (30 seconds). Importantly, the resistivity becomes nonzero during the pulse, indicating that the sample is heated back into the normal state. The sample is then allowed to cool back to the current base temperature, which is the indicated temperature in Figs. 1(c) and 1(d). Next, the PKE of the sample was measured for several minutes at the current base temperature using 10–20 μW of optical power. This is the region in Fig. 1(b) where $V_{2\omega}$ is nearly 30 mV and the sample resistance remains zero. This process was repeated as the base temperature of the system increased until the system warmed above T_c to approximately 3 K.

In field-cooled, zero-field-warmed measurements (ii), the sample was cooled in a constant magnetic field. After performing the demagnetization step needed to cool the system to base temperature, the indicated field was applied to the sample. A high-intensity laser pulse was then used to temporarily heat the sample above T_c without significantly raising the temperature of the base system. During the pulse, the sample temperature increased above T_c , which was confirmed by measuring the resistivity change in the sample. This process ensured that the sample cooled through T_c in the intended field and was not affected by the stray field from the demagnetization process. After the

single heat pulse, the field was set to zero, and the sample was warmed at a fixed rate by controlling the base temperature of the system. Measurements were typically made using 10 – 20 μW of incident optical power as the sample was warmed. A small offset was subtracted from each curve so that the mean of θ_K was zero for $T > T_c$. This offset is from a small remanent field ($< \pm 5$ Oe) that arises from the trapped flux in the demagnetization and sample-space superconducting magnets. Because the relationship between θ_K and the remanent field is known for $T > T_c$, it can be used to confirm the small magnitude of the remanent field.

Samples S1–S4 were prepared for optical measurements by polishing the surface. The Supplemental Material [26] also contains data on sample S8, which had as-grown surfaces that were suitable for optical measurements without polishing. No notable differences were observed in the measurements between the as-grown and polished surfaces. Additional heat pulse experiments were performed on S8 for which a local resistive heater was used to heat the sample above T_c instead of the laser. This allowed for the sample to cool from above T_c back to the base temperature over a period of 60 seconds instead of a few seconds. No differences related to the cooling rate were observed.

ACKNOWLEDGMENTS

Work at Los Alamos was primarily supported by the U.S. Department of Energy, Office of Basic Energy Sciences, Division of Materials Science and Engineering project “Quantum Fluctuations in Narrow-Band Systems.” Development of the Kerr effect capability was supported by the Los Alamos Laboratory Directed Research and Development program. M. M. B. and B. M. acknowledge support from the Los Alamos Laboratory Directed Research and Development program.

-
- [1] Manfred Sigrist and Kazuo Ueda, *Phenomenological theory of unconventional superconductivity*, *Rev. Mod. Phys.* **63**, 239 (1991).
- [2] Catherine Kallin and John Berlinsky, *Chiral superconductors*, *Rep. Prog. Phys.* **79**, 054502 (2016).
- [3] Masatoshi Sato and Yoichi Ando, *Topological superconductors: A review*, *Rep. Prog. Phys.* **80**, 076501 (2017).
- [4] Andrew P. Mackenzie, Thomas Scaffidi, Clifford W. Hicks, and Yoshiteru Maeno, *Even odder after twenty-three years: The superconducting order parameter puzzle of Sr_2RuO_4* , *npj Quantum Mater.* **2**, 40 (2017).
- [5] A. Pustogow, Yongkang Luo, A. Chronister, Y. S. Su, D. A. Sokolov, F. Jerzembeck, A. P. Mackenzie, C. W. Hicks, N. Kikugawa, S. Raghunath, E. D. Bauer, and S. E. Brown, *Constraints on the superconducting order parameter in Sr_2RuO_4 from oxygen-17 nuclear magnetic resonance*, *Nature (London)* **574**, 72 (2019).
- [6] Sheng Ran, Chris Eckberg, Qing-Ping Ding, Yuji Furukawa, Tristin Metz, Shanta R. Saha, I-Lin Liu, Mark Zic, Hyunsoo Kim, Johnpierre Paglione, and Nicholas P. Butch, *Nearly ferromagnetic spin-triplet superconductivity*, *Science* **365**, 684 (2019).
- [7] Lin Jiao, Sean Howard, Sheng Ran, Zhenyu Wang, Jorge Olivares Rodriguez, Manfred Sigrist, Ziqiang Wang, Nicholas P. Butch, and Vidya Madhavan, *Chiral superconductivity in heavy-fermion metal UTe_2* , *Nature (London)* **579**, 523 (2020).
- [8] Seokjin Bae, Hyunsoo Kim, Yun Suk Eo, Sheng Ran, I-lin Liu, Wesley T. Fuhrman, Johnpierre Paglione, Nicholas P. Butch, and Steven M. Anlage, *Anomalous normal fluid response in a chiral superconductor UTe_2* , *Nat. Commun.* **12**, 2644 (2021).
- [9] Kota Ishihara, Masaki Roppongi, Masayuki Kobayashi, Kumpei Imamura, Yuta Mizukami, Hironori Sakai, Petr Opletal, Yoshifumi Tokiwa, Yoshinori Haga, Kenichiro Hashimoto, and Takasada Shibauchi, *Chiral superconductivity in UTe_2 probed by anisotropic low-energy excitations*, *Nat. Commun.* **14**, 2966 (2023).
- [10] Robert Joynt and Louis Taillefer, *The superconducting phases of UPt_3* , *Rev. Mod. Phys.* **74**, 235 (2002).
- [11] E. R. Schemm, W. J. Gannon, C. M. Wishne, W. P. Halperin, and A. Kapitulnik, *Observation of broken time-reversal symmetry in the heavy-fermion superconductor UPt_3* , *Science* **345**, 190 (2014).
- [12] K. E. Avers, W. J. Gannon, S. J. Kuhn, W. P. Halperin, J. A. Sauls, L. DeBeer-Schmitt, C. D. Dewhurst, J. Gavilano, G. Nagy, U. Gasser, and M. R. Eskildsen, *Broken time-reversal symmetry in the topological superconductor UPt_3* , *Nat. Phys.* **16**, 531 (2020).
- [13] Ian M. Hayes, Di S. Wei, Tristin Metz, Jian Zhang, Yun Suk Eo, Sheng Ran, Shanta R. Saha, John Collini, Nicholas P. Butch, Daniel F. Agterberg, Aharon Kapitulnik, and Johnpierre Paglione, *Multicomponent superconducting order parameter in UTe_2* , *Science* **373**, 797 (2021).
- [14] Di S. Wei, David Saykin, Oliver Y. Miller, Sheng Ran, Shanta R. Saha, Daniel F. Agterberg, Jörg Schmalian, Nicholas P. Butch, Johnpierre Paglione, and Aharon Kapitulnik, *Interplay between magnetism and superconductivity in UTe_2* , *Phys. Rev. B* **105**, 024521 (2022).
- [15] Priscila F. S. Rosa, Ashley Weiland, Shannon S. Fender, Brian L. Scott, Filip Ronning, Joe D. Thompson, Eric D. Bauer, and Sean M. Thomas, *Single thermodynamic transition at 2K in superconducting UTe_2 single crystals*, *Commun. Mater.* **3**, 33 (2022).
- [16] A. Weiland, S. M. Thomas, and P. F. S. Rosa, *Investigating the limits of superconductivity in UTe_2* , *J. Phys.* **5**, 044001 (2022).
- [17] S. M. Thomas, C. Stevens, F. B. Santos, S. S. Fender, E. D. Bauer, F. Ronning, J. D. Thompson, A. Huxley, and P. F. S. Rosa, *Spatially inhomogeneous superconductivity in UTe_2* , *Phys. Rev. B* **104**, 224501 (2021).
- [18] D. Aoki, J.-P. Brison, J. Flouquet, K. Ishida, G. Knebel, Y. Tokunaga, and Y. Yanase, *Unconventional superconductivity in UTe_2* , *J. Phys. Condens. Matter* **34**, 243002 (2022).
- [19] Clément Girod, Callum R. Stevens, Andrew Huxley, Eric D. Bauer, Frederico B. Santos, Joe D. Thompson, Rafael M. Fernandes, Jian-xin Zhu, Filip Ronning, Priscila F. S. Rosa, and Sean M. Thomas, *Thermodynamic and electrical*

- transport properties of UTe₂ under uniaxial stress*, *Phys. Rev. B* **106**, L121101 (2022).
- [20] H. Sakai, P. Opletal, Y. Tokiwa, E. Yamamoto, Y. Tokunaga, S. Kambe, and Y. Haga, *Single crystal growth of superconducting UTe₂ by molten salt flux method*, *Phys. Rev. Mater.* **6**, 073401 (2022).
- [21] Dai Aoki, Hironori Sakai, Petr Opletal, Yoshifumi Tokiwa, Jun Ishizuka, Youichi Yanase, Hisatomo Harima, Ai Nakamura, Dexin Li, Yoshiya Homma, Yusei Shimizu, Georg Knebel, Jacques Flouquet, and Yoshinori Haga, *First observation of the de Haas-van Alphen effect and Fermi surfaces in the unconventional superconductor UTe₂*, *J. Phys. Soc. Jpn.* **91**, 1 (2022).
- [22] Luke Pritchard Cairns, Callum R. Stevens, Christopher D. O'Neill, and Andrew Huxley, *Composition dependence of the superconducting properties of UTe₂*, *J. Phys. Condens. Matter* **32**, 415602 (2020).
- [23] Shyam Sundar, Nasrin Azari, Mariah R. Goeks, Shayan Gheidi, Mae Abedi, Michael Yakovlev, Sarah R. Dunsiger, John M. Wilkinson, Stephen J. Blundell, Tristin E. Metz, Ian M. Hayes, Shanta R. Saha, Sangyun Lee, Andrew J. Woods, Roman Movshovich, Sean M. Thomas, Nicholas P. Butch, Priscila F. S. Rosa, Johnpierre Paglione, and Jeff E. Sonier, *Ubiquitous spin freezing in the superconducting state of UTe₂*, *Commun. Phys.* **6**, 24 (2023).
- [24] Jun Goryo, *Impurity-induced polar Kerr effect in a chiral p-wave superconductor*, *Phys. Rev. B* **78**, 060501(R) (2008).
- [25] Hao-Tian Liu, Weipeng Chen, and Wen Huang, *Impact of random impurities on the anomalous Hall effect in chiral superconductors*, *Phys. Rev. B* **107**, 224517 (2023).
- [26] See Supplemental Material at <http://link.aps.org/supplemental/10.1103/PhysRevX.13.041019> for additional experimental data and sample images.
- [27] Jing Xia, Peter T. Beyersdorf, M. M. Fejer, and Aharon Kapitulnik, *Modified Sagnac interferometer for high-sensitivity magneto-optic measurements at cryogenic temperatures*, *Appl. Phys. Lett.* **89**, 062508 (2006).
- [28] Charles P. Bean, *Magnetization of high-field superconductors*, *Rev. Mod. Phys.* **36**, 31 (1964).
- [29] John R. Clem and Zhidong Hao, *Theory for the hysteretic properties of the low-field dc magnetization in type-II superconductors*, *Phys. Rev. B* **48**, 13774 (1993).
- [30] C. Paulsen, G. Knebel, G. Lapertot, D. Braithwaite, A. Pourret, D. Aoki, F. Hardy, J. Flouquet, and J.-P. Brison, *Anomalous anisotropy of the lower critical field and Meissner effect in UTe₂*, *Phys. Rev. B* **103**, L180501 (2021).
- [31] Satyajit Banerjee, *Nonlinear response of the static and dynamic phases of the vortex matter*, in *Superconductivity—Theory and Applications*, edited by Adir Moyses Luiz (IntechOpen, London, 2011), Chap. 4, pp. 55–84, 10.5772/684.
- [32] Adrien Rosuel, Christophe Marcenat, Georg Knebel, Thierry Klein, Alexandre Pourret, Nils Marquardt, Qun Niu, Simon Rousseau, Albin Demuer, Gabriel Seyfarth, Gérard Lapertot, Dai Aoki, Daniel Braithwaite, Jacques Flouquet, and J. P. Brison, *Field-induced tuning of the pairing state in a superconductor*, *Phys. Rev. X* **13**, 011022 (2023).
- [33] Z. Koziol, J. J. M. Franse, P. F. de Chatel, and A. A. Menovsky, *Magnetization of a superconductor: Results from the critical-state model*, *Phys. Rev. B* **50**, 15978 (1994).
- [34] E. R. Schemm, R. E. Baumbach, P. H. Tobash, F. Ronning, E. D. Bauer, and A. Kapitulnik, *Evidence for broken time-reversal symmetry in the superconducting phase of URu₂Si₂*, *Phys. Rev. B* **91**, 140506(R) (2015).
- [35] Yusuke Iguchi, Huiyuan Man, S. M. Thomas, Filip Ronning, Priscila F. S. Rosa, and Kathryn A. Moler, *Microscopic imaging homogeneous and single phase superfluid density in UTe₂*, *Phys. Rev. Lett.* **130**, 196003 (2023).
- [36] Sirak M. Mekonen, Chang-Jong Kang, Dipanjan Chaudhuri, David Barbalas, Sheng Ran, Gabriel Kotliar, Nicholas P. Butch, and N. P. Armitage, *Optical investigation of the heavy-fermion normal state in superconducting UTe₂*, *Phys. Rev. B* **106**, 085125 (2022).
- [37] Florian Theuss, Avi Shragai, Gael Grissonnanche, Ian M. Hayes, Shanta R. Saha, Yun Suk Eo, Alonso Suarez, Tatsuya Shishidou, Nicholas P. Butch, Johnpierre Paglione, and B. J. Ramshaw, *Single-component superconductivity in UTe₂ at ambient pressure*, [arXiv:2307.10938](https://arxiv.org/abs/2307.10938).
- [38] N. Azari, M. Yakovlev, N. Rye, S. R. Dunsiger, S. Sundar, M. M. Bordelon, S. M. Thomas, J. D. Thompson, P. F. S. Rosa, and J. E. Sonier, *Absence of spontaneous magnetic fields due to time-reversal symmetry breaking in bulk superconducting UTe₂*, [arXiv:2308.09773](https://arxiv.org/abs/2308.09773).
- [39] Petr Opletal, Hironori Sakai, Yoshinori Haga, Yoshifumi Tokiwa, Etsuji Yamamoto, Shinsaku Kambe, and Yo Tokunaga, *Ferromagnetic crossover within the ferromagnetic order of U₇Te₁₂*, *J. Phys. Soc. Jpn.* **92**, 1 (2023).
- [40] O. Tougait, G. André, F. Bourée, and H. Noël, *Neutron diffraction study of magnetic ordering of two binary uranium tellurides U₃Te₅ and U₂Te₃*, *J. Alloys Compd.* **317–318**, 227 (2001).
- [41] Alexander Fried, Martin Fejer, and Aharon Kapitulnik, *A scanning, all-fiber Sagnac interferometer for high resolution magneto-optic measurements at 820 nm*, *Rev. Sci. Instrum.* **85**, 103707 (2014).
- [42] Aharon Kapitulnik, Jing Xia, Elizabeth Schemm, and Alexander Palevski, *Polar Kerr effect as probe for time-reversal symmetry breaking in unconventional superconductors*, *New J. Phys.* **11**, 055060 (2009).
- [43] Sudeep Kumar Ghosh, Michael Smidman, Tian Shang, James F. Annett, Adrian D. Hillier, Jorge Quintanilla, and Huiqiu Yuan, *Recent progress on superconductors with time-reversal symmetry breaking*, *J. Phys. Condens. Matter* **33**, 033001 (2021).
- [44] Karol Izidor Wysokiński, *Time reversal symmetry breaking superconductors: Sr₂RuO₄ and beyond*, *Condens. Matter* **4**, 47 (2019).
- [45] Wen Huang, *A review of some new perspectives on the theory of superconducting Sr₂RuO₄*, *Chin. Phys. B* **30**, 107403 (2021).